International Journal of Heat and Mass Transfer 51 (2008) 5465–5474

Contents lists available at ScienceDirect

International Journal of Heat and Mass Transfer

journal homepage: www.elsevier.com/locate/ijhmt

Technical Note

A boundary layer analysis of electro-magneto-hydrodynamic forced convective transport over a melting slab

Suman Bose, Suman Chakraborty *

Department of Mechanical Engineering, Indian Institute of Technology, Kharagpur 721 302, India

ARTICLE INFO

Article history:
Received 3 July 2007
Received in revised form 18 February 2008
Available online 29 May 2008

ABSTRACT

In this work, a boundary layer based integral approach is employed for analyzing the coupled problem of electro-magneto-hydrodynamic convection and melting of an electrically conducting material. The melting process is assumed to occur on a semi-infinite flat horizontal slab. The simultaneous non-linear ordinary differential equations, originated out of the boundary layer analysis, are solved by employing the fourth order Runge–Kutta method, in a novel iterative framework. Simulation studies are executed for representative systems of materials, with a wide range of variation of processing parameters. Effects of melt superheat and the strengths of magnetic and electric fields on the melting process are analyzed in details. Fundamental physical principles are subsequently outlined for controlling the melting process through combined electrical and magnetic fields, on the employment of judicious combinations of the relevant operating parameters.

1. Introduction

The use of external magnetic and electric fields has now become widespread in the metal and semiconductor industries for controlling the transport phenomena during melting/solidification processes, resulting in improved processing capabilities and better product qualities. The electromagnetic fields may be configured to provide effective means of melt stirring, which is likely to be useful in generating a desired melt mixing pattern during semiconductor crystal growth or producing a strong turbulent shear flow to induce grain refinement effects during casting processes. A direct current magnetic field, on the other hand, may also be used to suppress undesirable turbulent fluctuations in melt flows, in order to minimize the manufacturing defects in certain applications. Keeping such wide-ranging implications in view, extensive research efforts have been directed towards developing a fundamental understanding on the physics of electro-magneto-hydrodynamic convective flows in molten materials and designing effective measures to control and optimize the pertinent materials processing operations.

The first attempt of deliberately employing magnetic fields to benefit materials processing operations involving melting/solidification dates back to the early 1930s [1,2]. At present, the use of magnetic fields has become a standard industrial practice in the solidification processing of electrically conducting fluids such as molten metals and semiconductors [3–5]. In general, the electromagnetic fields have been directed to satisfy a diverse set of requirements, ranging from the induction of melt convection deep in the solidifying liquid pool to the dampening of turbulence in melt convection. These effects have been explored in both metals and semiconductor industries, and the resulting improvements in both process control and product quality have been encouraging. In general, the application of magnetic fields has been shown to stabilize both flow and temperature oscillations in the melt [6], and thereby represents a promising opportunity to obtain an improved crystal quality. Keeping this perspective in view, the effects of a magnetic field on melt convection were numerically investigated by several authors, primarily focusing on the aspects of buoyancy- and surface tension-driven convection [7–11]. These studies, however, dealt primarily with the effects of a magnetic field on the fluid flow and did not include the effects of phase-change. Kaddeche et al. [12] presented a numerical study on macrosegregation in a horizontal Bridgman configuration under various fluid flow conditions and with the assumption of a planar solid–liquid interface moving at a constant velocity. Fedoseyev et al. [13] studied the transport phenomena associated with magnetic field suppression of semiconductor melt flow in crystal growth processes, and were amongst the first group of researchers to clearly detail the boundary layer formation near rigid walls under those conditions. It was revealed that sufficiently strong magnetic fields could significantly damp the convection in the melt, resulting in a planar solidification front.

The idea of utilizing combined electro-magneto-hydrodynamic (EMHD) influences in controlling melting/solidification processes has been a natural extension of the successful exploitation of magnetic fields in advanced materials processing applications [14–16], outlined as above. As such, it has been well known for decades that

* Corresponding author.
E-mail address: suman@mech.iitkgp.ernet.in (S. Chakraborty).

0017-9310/$ - see front matter © 2008 Elsevier Ltd. All rights reserved.
doi:10.1016/j.ijheatmasstransfer.2008.02.051

Nomenclature

a	coefficient in velocity profile
b	coefficient in temperature profile
B_o	magnetic field strength, A m^{-1}
C_p	specific heat, J kg^{-1} K^{-1}
D	melting parameter
e	square root of the ratio of dimensionless electric field strength to Ec Eckert number
E	dimensionless electric field strength
E_o	electric field strength, kg m s^{-3} A^{-1}
Ec	Eckert number
$\hat{i}$, $\hat{j}$, $\hat{k}$	unit vectors in x-, y-, z-directions respectively
H	latent heat of liquid/solid phase transformation, J kg^{-1}
H_t	Hartmann number
J	electric current density, A m^{-2}
k	thermal conductivity, W m^{-1} K^{-1}
L	characteristic length of the plate in x-direction, m
M	dimensionless magnetic field strength
$\overline{m}$	melt generation rate per unit area, kg s^{-1} m^{-2}
Nu	Nusselt number
Pe	Peclet number
Pr	Prandtl number
Re	Reynolds number
Ste	Stefan number
$\overline{T}$, T	dimensional and dimensionless temperature
$\overline{U}$, U	dimensional and dimensionless horizontal velocity component
$\overline{V}$, V	dimensional and dimensionless vertical velocity component
v	velocity vector of flow
$\bar{x}$, x	dimensional and dimensionless axial coordinate
$\bar{y}$, y	dimensional and dimensionless vertical coordinate

Greek symbols

α	thermal diffusivity, m^2 s^{-1}
$\bar{\delta}$, δ	dimensional and dimensionless boundary layer thickness
Δ	ratio of thermal to momentum (hydrodynamic) boundary layer thickness
η	normalized coordinate with respect to hydrodynamic boundary layer thickness
κ	ratio of liquid to solid thermal conductivity
λ	ratio of maximum temperature difference in solid to that in liquid
ν	kinematic viscosity, m^2 s^{-1}
ω	normalized coordinate with respect to δt
ζ	normalized interfacial velocity
ρ	mass density, kg m^{-3}
σ	electrical conductivity, S m^{-1}

Subscripts

f, F	liquid phase, melt surface
o	condition in solid at infinite distance from the melting interface
∞	free stream condition
m	momentum (hydrodynamic) boundary layer
s	solid phase
t	thermal boundary layer

Superscript

0	parameter in absence of electro-magnetic field

fluid flow, and hence convective heat transfer, could be significantly influenced if an electrically conducting fluid is subjected to combined electro-magnetic influences. However, detailed mathematical models on the interaction of the electric, magnetic, thermal, gravitational and pressure fields have not been reported in the literature, till recent times [16–19]. In fact, the complete EMHD models in the context of melting/solidification transport have been solved in the literature only for a restricted class of problems. A major subclass of the EMHD models employed for the analysis of melting/solidification problems in the literature has either concerned with incompressible fluid flows under the influence of an externally imposed magnetic field alone, while neglecting any electric fields, or has concerned with incompressible fluid flows under the sole influence of an externally imposed electric field while neglecting the presence of any magnetic fields. Not only that, most of the above-mentioned studies have been based on full-scale numerical models, which often appear to be over-complicated in nature in providing fundamental insights into the strongly interconnected and somewhat non-trivial physical mechanisms that govern the influences of combined electro-magnetic fields on melting/solidification processes of conducting materials. Nevertheless, despite such complicated physical issues being involved, a number of interesting analytical or semi-analytical studies on the influence of magnetic fields on convective transport have also been reported in the literature. Most of these analytical investigations have been based on either the similarity techniques or the approximate integral methods [20–22]. It is interesting to mention here that these techniques have successfully been employed to independently study the melting heat transfer over flat plates [23,24], although without concerning the use of any magnetic or electric fields. Seeniraj and Kannan [25], for the first time, offered with an integral analysis of the coupled problem of hydromagnetic flow and melting of an electrically conducting liquid over a slab. For the convenience in mathematical analysis, they neglected the effects of Joule heating in formulating the energy conservation equation. In reality, however, such effects may turn out to be immensely critical, especially for the cases in which the superheat in the melt occurs to be relatively low. Moreover, their work did not consider the influence of any externally applied electric field, which, along with the magnetic field, might influence the resultant transport processes in a rather involved manner, with possible non-trivial implications on the rate of heat transfer associated with the melting process.

Aim of the present work is to devise a semi-analytical model based on the boundary layer integral method, for analyzing the combined effects of magnetic and electric fields on the melting of a flat horizontal slab, under the laminar forced flow of a conducting liquid. Besides their theoretical implications, such semi-analytical solutions hold their critical significance in a sense that these are likely to provide valuable detailed insights on the characteristics of the overall solution, without necessitating involved computational efforts. Not only that, such semi-analytical solutions can also be utilized to check the accuracy, convergence and effectiveness of various full-scale numerical computation methods and to improve their differencing schemes, grid generation ways and so on. Keeping this in perspective, a simplified mathematical model is considered in the present study, by considering identical thermo-physical properties in solid and liquid phases. The coupled boundary layer equations are obtained by employing the von Karmann approximate integral approach, and the resultant non-linear systems of or-

dinary differential equations are solved by employing simple numerical schemes.

2. Mathematical modeling

2.1. Model description and problem formulation

The physical situation addressed in the present analysis deals with a model problem, as schematically depicted in Fig. 1. As shown in the figure, the free stream flow of a molten pure material takes place over a solid layer of the same, with no imposed pressure gradients in the fluid. The free stream velocity and temperature of the liquid are $\overline{U}_\infty$ and $\overline{T}_\infty$, respectively, and the bulk temperature of the solid is $\overline{T}_s$. At steady state, the interface is at the melting temperature of the material ($\overline{T}_f$). The solid melts at a constant rate of $\overline{V}_F$ locally, due to the hot fluid flowing over it. This continuous depletion of solid is adjusted by feeding un-melted material at a local rate of $\overline{V}_s$ from the bottom. A magnetic field of strength B_o is imposed along y-direction, while an electric field of strength E_o is imposed orthogonal to the magnetic field and to the flow direction.

For mathematical analysis, the following major assumptions are made:

(1) The liquid is weakly conducting and does not carry any free charge.
(2) The strengths of the magnetic and electric fields are constants. Further, the solid medium is considered to be of semi-infinite extent, following the works of the earlier researchers. Because of this, the volumetric heat generation (i.e., the rate of heat generation per unit volume) in the solid tends to zero in a limiting sense, consistent with the mathematical model considered here. In practice, any heat generation within the solid of finite extent will merely serve to increase the bulk temperature, or for that matter the temperature gradient inside the solid, without disturbing the other aspects of the present model.
(3) Thermo-electric effects like Peltier and Seeback effects are neglected.
(4) The flow is two dimensional, laminar, steady and incompressible.
(5) Induced magnetic and electric fields are negligible in strength.
(6) The thermo-physical properties of the material are constant.

Since the problem involves a combination of electric and magnetic fields, a unified EMHD theory [17] is employed to derive the governing differential equations. The original form of the equations is involved and is not presented here. The simplified forms, obtained after applying the assumptions mentioned as above, are presented below:

1. *Continuity equation*

$$\nabla \cdot \vec{v} = 0 \tag{1}$$

where $\vec{v}$ is the velocity at any point in the liquid, given by $\vec{v} = \overline{U}\hat{i} + \overline{V}\hat{j}$.

2. *Momentum equation*

$$\rho(\vec{v}\cdot\nabla)\vec{v} = -\nabla P + \mu\nabla^2\vec{v} + (\vec{J}\times\vec{B}) \tag{2}$$

where $(\vec{J}\times\vec{B})$ is the electromagnetic (Lorentz) force vector, which is a combined consequence of the magnetic field ($\vec{B} = B_o\hat{j}$) and the electric field ($\vec{E} = E_o\hat{k}$). The net electromotive vector is given by $\vec{\varepsilon} = \vec{E} + \vec{v}\times\vec{B}$, which on simplification becomes $\vec{\varepsilon} = (E_o + \overline{U}\times B_o)\hat{k}$, so that the current density is obtained as $\vec{J} = \sigma\vec{\varepsilon}$.

3. *Energy equation*

$$(\vec{v}\cdot\nabla)T = \alpha\nabla^2 T + S \tag{3}$$

where $S = (\vec{J}\cdot\vec{\varepsilon})/\rho C_{pf}$.

Eqs. (1)–(3) are further simplified by employing the standard boundary layer assumptions, and are subsequently non-dimensionalized by employing the following normalization parameters (various symbols are explained in the Nomenclature section):

$$x = \frac{\bar{x}}{L},\quad y = \frac{\bar{y}}{L},\quad \delta_m = \frac{\bar{\delta}_m}{L},\quad \delta_t = \frac{\bar{\delta}_t}{L},\quad \Delta = \frac{\delta_t}{\delta_m},\quad \omega = \frac{y}{\delta_t},$$

$$\eta = \frac{y}{\delta_m},\quad U = \frac{\overline{U}}{\overline{U}_\infty},\quad V = \frac{\overline{V}}{\overline{V}_F},\quad \zeta = \frac{\overline{V}_F}{\overline{U}_\infty},\quad \theta = \frac{\overline{T}-\overline{T}_f}{\overline{T}_\infty-\overline{T}_f},$$

$$\theta_s = \frac{\overline{T}_s-\overline{T}_o}{\overline{T}_f-\overline{T}_o},\quad \lambda = \frac{\overline{T}_\infty-\overline{T}_f}{\overline{T}_f-\overline{T}_o},\quad Re = \frac{\overline{U}_\infty L}{\nu_f},\quad Pr = \frac{\nu_f}{\alpha_f},$$

$$Pe = Re\cdot Pr,\quad Nu_x = \frac{h\bar{x}}{k_f},\quad Ste_f = \frac{Cp_f(\overline{T}_\infty-\overline{T}_f)}{H},$$

$$Ste_s = \frac{Cp_s(\overline{T}_f-\overline{T}_o)}{H},\quad D = \frac{Ste_f}{1+Ste_s},\quad Ec = \frac{\overline{U}_\infty^2}{Cp_f(\overline{T}_\infty-\overline{T}_f)} = \frac{\overline{U}_\infty^2}{H}\times\frac{1}{Ste_f},$$

$$\kappa = \frac{k_f}{k_s},\quad M = B_o L\sqrt{\frac{\sigma_f}{\mu}}\frac{1}{\sqrt{Re}} = \frac{H_t}{\sqrt{Re}},$$

$$E = E_o\sqrt{\frac{\sigma_f L}{\overline{U}_\infty\rho Cp_f(\overline{T}_\infty-\overline{T}_f)}} = E_o\sqrt{\frac{\sigma_f L}{\overline{U}_\infty\rho H}}\sqrt{\frac{1}{Ste_f}}$$

Using the above non-dimensional numbers, the governing differential equations for the momentum and the thermal boundary layers become:

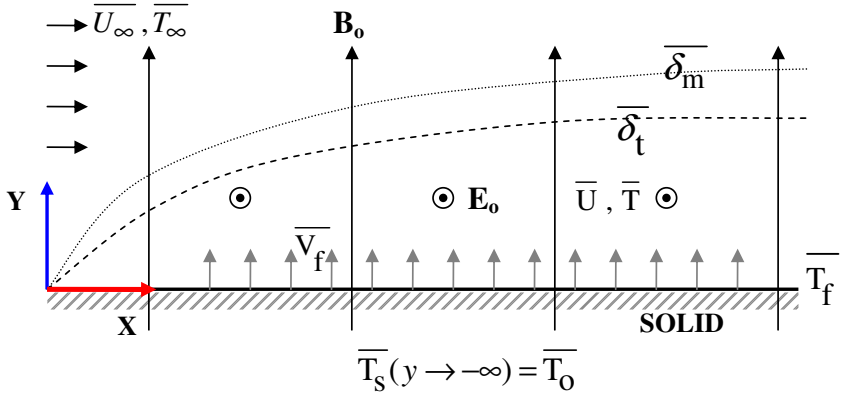

Fig. 1. Schematic diagram of the problem (electric field is in z-direction).

1. *Continuity*

$$\frac{\partial U}{\partial x}+\zeta\frac{\partial V}{\partial y}=0 \tag{4}$$

2. *Momentum*

$$U\frac{\partial U}{\partial x}+\zeta V\frac{\partial U}{\partial y}=\frac{1}{Re}\frac{\partial^2 U}{\partial y^2}+M^2(1-U) \tag{5}$$

3. *Energy*

$$U\frac{\partial \theta}{\partial x}+\zeta V\frac{\partial \theta}{\partial y}=\frac{1}{Pe}\frac{\partial^2 \theta}{\partial y^2}+(E+U\cdot M\sqrt{Ec})^2 \tag{6}$$

It may be noted here that although the electric field produces a body force on the fluid, the same does not show up in the momentum equation because it is constant, and can be eliminated by suitably defining a modified pressure. The only external force that affects the fluid motion is the electromagnetic (Lorentz) force. In the energy equation, the source term represents the effects of Joule heating caused by the flow of current due to the imposed electric field and also the current generated due to the magnetic flux. The above system of equations is consistent with the following interfacial energy balance condition:

$$k_f\left.\frac{\partial T}{\partial y}\right|_{y=0^+}=H\rho_f V_F+k_s\left.\frac{\partial T}{\partial y}\right|_{y=0^-} \tag{7}$$

It can also be noted here that in the absence of any electric field in the solid, the solution of the temperature distribution in the solid may be derived according to the procedure outlined in [25], to yield

$$\theta_s=\exp\left(\kappa\lambda\frac{Ste_s}{Ste_f}Pe\zeta y\right)\quad \text{for } -\infty\leqslant y\leqslant 0 \tag{8}$$

For obtaining the temperature distribution in the liquid, an integral analysis is performed, involving the systems of Eqs. (4)–(7), as presented in the subsequent section.

2.2. Integral analysis

For deriving the solutions by employing the boundary layer integral method, the governing differential equations (4)–(6) are first integrated inside their respective boundary layers, to obtain their corresponding integral forms, as

$$\zeta(V-1)=\int_0^{\delta_m}\frac{\partial U}{\partial x}\,dy \tag{9}$$

$$\frac{d}{dx}\left(\int_0^{\delta_m}U(1-U)\,dy\right)-\zeta=\frac{1}{Re}\left.\frac{\partial U}{\partial y}\right|_{y=0}-\int_0^{\delta_m}(1-U)M^2\,dy \tag{10}$$

$$\frac{d}{dx}\left(\int_0^{\delta_t}U(1-\theta)\,dy\right)-\zeta=\frac{1}{Pe}\left.\frac{\partial \theta}{\partial y}\right|_{y=0}-\int_0^{\delta_t}\left(E+UM\sqrt{Ec}\right)^2 dy \tag{11}$$

For evaluating the integrals appearing in Eqs. (9)–(11), the dimensionless velocity and temperature profiles within the boundary layer are first approximated as

$$U(\eta)=a_0+a_1\eta+a_2\eta^2+a_3\eta^3 \tag{12a}$$

$$\theta(\eta)=b_0+b_1\omega+b_2\omega^2+b_3\omega^3 \tag{12b}$$

The pertinent boundary conditions on velocity are as follows:

$$U(0)=0,\quad U(1)=1,\quad \left.\frac{\partial U}{\partial \eta}\right|_{\eta=1}=0,$$

$$D\left.\frac{\partial \theta}{\partial \omega}\right|_{\omega=0}\left.\frac{\partial U}{\partial \eta}\right|_{\eta=0}=\Delta Pr\left.\frac{\partial^2 U}{\partial \eta^2}\right|_{\eta=0}+M^2Pe\Delta\delta_m^2 \tag{13a–d}$$

The boundary condition given by Eq. (13d) has been derived by noting that Eq. (5) needs also to be satisfied at the solid/liquid interface, in conjunction with Eq. (7). Similarly, the boundary conditions for temperature can be derived from Eqs. (6) and (7), to yield

$$\theta(0)=0,\quad \theta(1)=1,\quad \left.\frac{\partial \theta}{\partial \omega}\right|_{\omega=1}=0,$$

$$D\left[\left.\frac{\partial \theta}{\partial \omega}\right|_{\omega=0}\right]^2=\left.\frac{\partial^2 \theta}{\partial \omega^2}\right|_{\omega=0}+EPe\Delta\delta_t^2 \tag{14a–d}$$

Using the boundary conditions (13) and (14), various coefficients appearing in Eq. (12) are obtained as

$$a_0=0,\quad a_1=\phi(6+M^2Re\delta_m^2),\quad a_2=3-2a_1,\quad a_3=a_1-2 \tag{15a–d}$$

$$b_0=0,\quad b_1=\frac{2}{D}\left(\sqrt{1+\frac{3}{2}D+\frac{DPe\{E\Delta\delta_m\}^2}{4}}-1\right),$$

$$b_2=3-2b_1,\quad b_3=b_1-2 \tag{16a–d}$$

where $\phi=\frac{\Delta Pr}{Db_1+4\Delta Pr}$. The expression for the dimensionless interfacial velocity, ζ, can be found out by using Eqs. (7) and (12), which on rearrangement, yields

$$\zeta=\frac{b_1 D}{Pe\Delta\delta_m} \tag{17}$$

Expression (12a), along with the coefficients specified by Eq. (15d), can subsequently be employed to evaluate the integrals appearing in Eqs. (9) and (10), to obtain an ordinary differential equation of the following form:

$$\frac{d}{dx}[c_1\delta_m+c_2\delta_m^2+c_3\delta_m^3]=\frac{1}{Re\delta_m}\left[6\phi+\frac{Db_1}{\Delta Pr}\right]+\frac{M^2\delta_m}{2}(\phi+1)+\frac{1}{12}M^4Re\delta_m^3\phi \tag{18}$$

The parameters c_1, c_2, c_3, as appearing in Eq. (18), are detailed in Appendix A.

Unlike the momentum equation, the energy equation cannot be integrated in a trivial and straight forward manner. This is because of the fact that a disparate thermal behavior characterizes high Prandtl number and low Prandtl number fluids, on account of the distinctive relative thicknesses of the momentum and the thermal boundary layer in the two cases. These two limiting cases, therefore, are addressed separately in the subsequent sections.

2.2.1. Case 1: $Pr\gg 1$ ($\Delta\ll 1$)

For liquids with Prandtl number much greater than unity ($Pr\gg 1$), the momentum boundary layer is substantially thicker than the thermal boundary layer. Under these conditions, the velocity profile given by Eq. (12a) can be considered to prevail over the entire span of the thermal boundary layer, so that Eq. (11) yields

$$\frac{d}{dx}[c_1\delta_m+c_2\delta_m^2]=\frac{b_1(1+D)}{Pe\Delta\delta_m}+Ec[d_1\delta_m+d_2\delta_m^3+d_3\delta_m^5] \tag{19}$$

On defining additional parameters e such that $e=\sqrt{\frac{E}{Ec}}$, the terms c_1, c_2, d_1, d_2, d_3, as appearing in Eq. (19), can be completely specified, as detailed in Appendix A.

2.2.2. Case 2: $Pr\ll 1$ ($\Delta\gg 1$)

For liquids with low Prandtl number ($Pr\ll 1$), the momentum boundary layer is much thinner in comparison to the thermal boundary layer. As a consequence, the velocity profile given by Eq. (12a) prevails only over a small portion of the thermal boundary layer, outside which the velocity is effectively same as the free stream velocity. Taking this fact into consideration, Eq. (11) yields

$$\frac{d}{dx}[c_1\delta_m+c_2\delta_m^2]=\frac{b_1(1+D)}{Pe\Delta\delta_m}+Ec[d_1\delta_m+d_2\delta_m^3+d_3\delta_m^5] \tag{20}$$

The parameters c_1, c_2, d_1, d_2, d_3, as appearing in Eq. (20), are detailed in Appendix A.

2.3. Numerical considerations and post-processing

The coupled non-linear ordinary differential equations governing the variations of δ_m and Δ (as given by Eqs. (18) and (19)/(20)) are numerically solved by employing the shooting technique. The boundary value problem is converted into a system of initial value problems, which is solved by employing the fourth order Runge–Kutta method. The non-linear algebraic variations of the dependent variables at each step are handled by employing an iterative error minimization approach, without involving any derivative calculations. This approach is rather insensitive to the choice of the initial guess, and is found to yield converged solutions, within a relative error tolerance of as small as 10^{-6}. From the variations of δ_m and Δ, the melt generation rate can be found out as $\dot{\overline{m}} = \zeta\rho_f$, where the parameter ζ may be calculated using Eq. (17). Another important parameter, which gives a quantitative estimate of the strength of convective heat transfer, is the Nusselt number. The local Nusselt number is defined as $Nu_x = \frac{x}{\delta_f}\frac{\partial\theta}{\partial\omega}\big|_{\omega=0} = \frac{xb_1}{\Delta\delta_m}$. The ratio of the local Nusselt number obtained with and without the electromagnetic fields can be described as

$$\frac{Nu_x}{Nu_x^0} = \frac{xb_1}{\Delta\delta_m Nu_x^0} \tag{21}$$

This ratio is of immense practical significance, since it assesses the effectiveness of the electrical and the magnetic fields on the overall rate of heat transfer associated with the melting process. In the numerical implementation, initially the results are generated without the applied fields to get Nu_x^0. Then the external electro-magnetic field is applied and the new results are obtained. At each location Nu_x is divided by Nu_x^0 obtained from the previous results to obtain the ratio of Nusselt numbers.

3. Results and discussion

Apart from the material properties, the three major parameters which govern the behavior of melting are the degree of liquid superheat $\overline{T}_\infty - \overline{T}_f$, the strength of electric field (E_o), and the strength of magnetic field (B_o). The effects of these parameters are studied for both high and low Prandtl number liquids, in terms of the effects of the corresponding non-dimensional numbers on the melting behavior.

3.1. Model validation

Results from the present model are first validated against the numerical results reported by Seeniraj and Kannan [25]. However, since these authors considered the effects of magnetic field alone without involving any electrical field, the electric field strength (E) employed in the present study is set to zero, so as to render the results from the two studies effectively comparable. The comparison is shown in Fig. 2, which shows a fairly good agreement between the two model predictions. It is interesting to note that there is a perceptible (although minor) deviation between the two predictions, for non-zero strengths of the magnetic field. This can be attributed to the fact that the analysis of Seeniraj and Kannan [25] neglected the Joule heating effects, while those are aptly accounted for in the present model. Although these effects may be rather of limited consequence in presence of a magnetic field alone, these may indeed turn out to be of significant consequence in presence of combined electro-magneto-hydrodynamic influences, as evidenced from our subsequent analysis.

With the preliminary assessment of the model in presence of magnetic fields alone, simulation studies are subsequently executed to bring out the combined consequences of the electrical and the magnetic fields on the overall melting process. These studies are discussed in details in the subsequent sections.

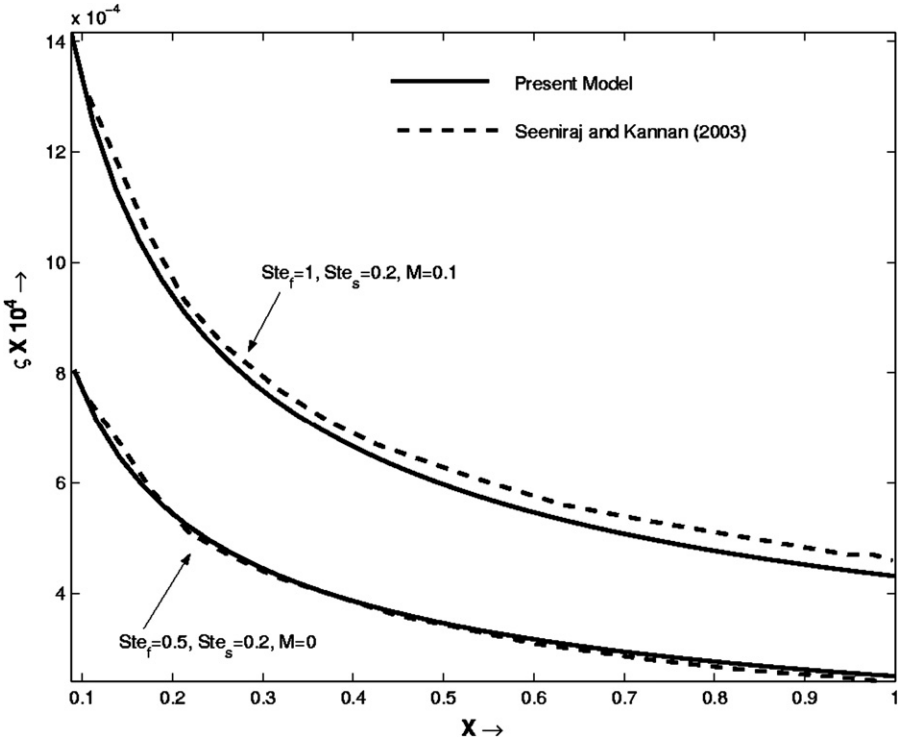

Fig. 2. Comparison of values of the non-dimensional interfacial velocity, ζ, as calculated from the present model with the results reported by Seeniraj and Kannan [25].

Table 1
Numerical values of non-dimensional parameters (unless mentioned)

Parameter	Numerical value
Re	10,000
Ste_s	1
Ste_f	1
Pr	100 ($Pr \gg 1$) 0.001 ($Pr \ll 1$)
$\frac{U_\infty^2}{H}$	1
$E_0\sqrt{\frac{\sigma_f L}{U_\infty \rho H}}$	0.3
H_t	30

3.2. Case studies with combined electro-magneto-hydrodynamic influences

3.2.1. Effect of liquid superheat with combined electro-magnetic fields

The effect of variations in the degree of superheat is studied by varying Ste_f, since they are directly proportional to each other. The numerical values of the different parameters used to execute this analysis are listed in Table 1. Fig. 3 demonstrates the effect of the degree of superheat in the liquid on various aspects of the melting process, for $Pr \gg 1$. It can be seen (refer to Fig. 3a–c) that an increase in the degree of superheat does not affect the ratio of the thermal to momentum boundary layer thickness (Δ) or the momentum boundary layer thickness (δ_m), but enhances the rate of melting (ζ). It is important to note in this context that the thermal boundary layer thickness is a combined consequence of the competing influences of the thermal advection and transverse diffusion, for a given rate of thermal energy generation (Joule heating). Since both the advective and diffusive effects scale linearly with the degree of superheat, the thermal boundary layer thickness is virtually unaffected with a change in the degree of superheat. With an added superheat, however, a major proportion of the heat flux available to the liquid gets consumed in the form of latent heat, as a consequence of an enhanced rate of melting. The plot of the ratio of Nusselt numbers (see Fig. 3d) shows that the Nusselt number remains virtually unaffected with degree of superheat. However, its increasing trend along axial direction suggests that the effect of the electro-magnetic field becomes more prominent as one moves away from the leading edge of the slab. The ratio of the Nusselt number with and without electro-magnetic field can be expressed as $(\delta_t^0/\delta_t)(b_1/b_1^0)$. While the ratio (b_1/b_1^0) is hardly affected by electro-magnetic field, the ratio (δ_t^0/δ_t) increases with increase in the strength of the electro-magnetic field. This is because of the fact that enhanced electromagnetic field strength causes more heat generation within the boundary layer, thereby decreasing the magnitude of δ_t. At the leading edge, there is virtually no heat generation, and accordingly the ratio of Nusselt numbers becomes almost same as unity. However, as we move away from the leading edge, the effect of the electro-magnetic field becomes progressively more pronounced, and the ratio of Nusselt numbers consequently increases. However, neither b_1 nor δ_t is affected by degree of superheat, which explains the fact that the ratio of Nusselt numbers remain unaffected by degree of superheat.

Fig. 4 depicts similar variations as those exhibited in Fig. 3, but for the case of $Pr \ll 1$. Since the influences of the degree of superheat are not very much related to the relative magnitudes of the momentum and thermal diffusivities, the variations in boundary layer thickness, melting rate, and the Nusselt number are observed to be virtually identical in a qualitative sense for both cases of high and low Prandtl number fluids, as observed by comparing Figs. 3 and 4. However, the distinctive influences of high and low Prandtl number fluid become conspicuous with regard to the implications in the variations of the electrical and magnetic field strengths in certain aspects, to be discussed subsequently.

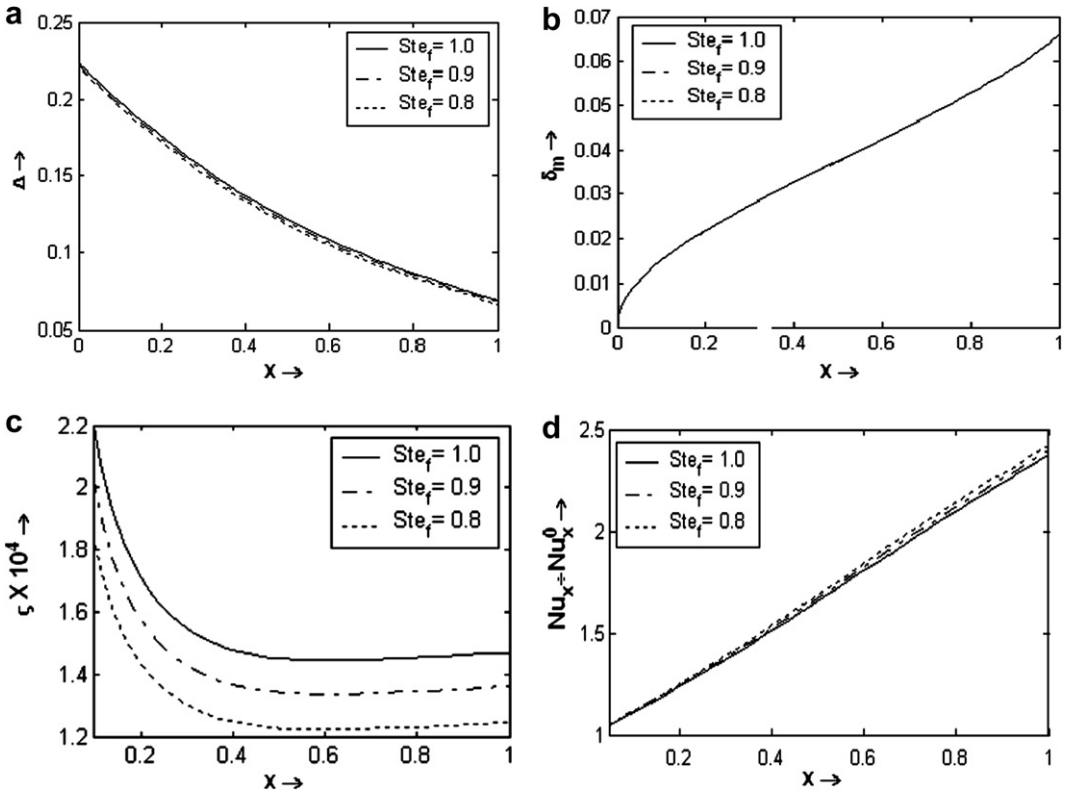

Fig. 3. Effect of degree of superheat for liquid of $Pr \gg 1$, on (a) Δ, (b) δ_m, (c) ζ, (d) ratio of Nu_x to Nu_x^0.

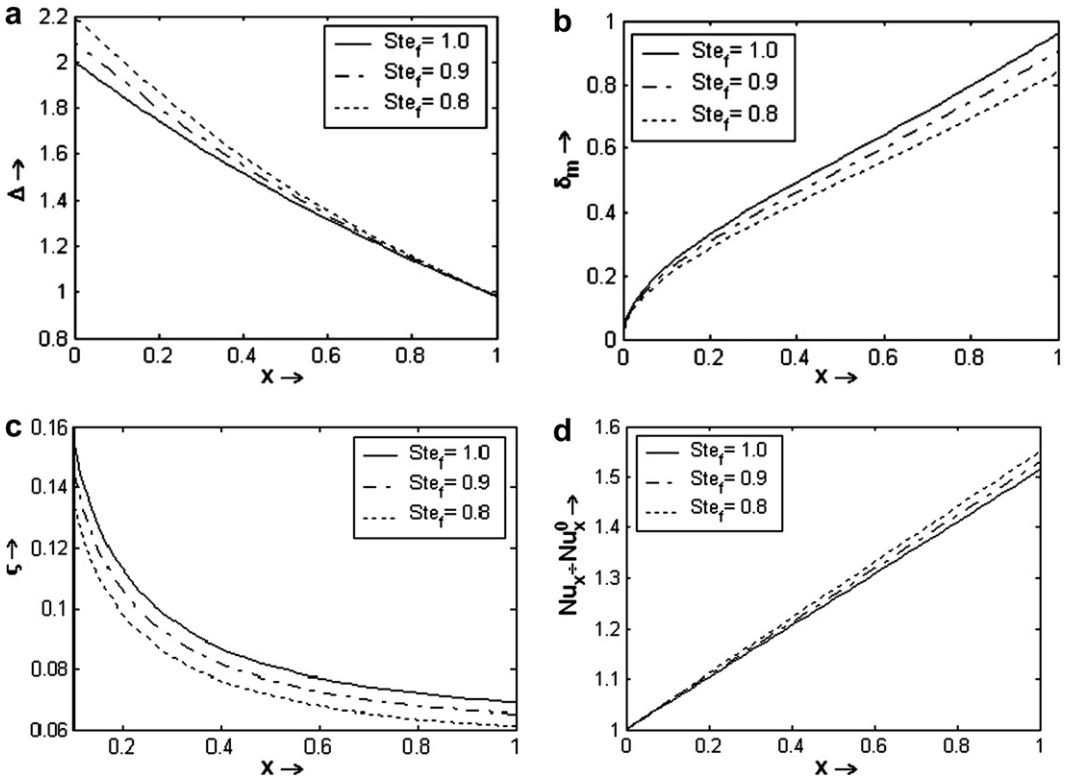

Fig. 4. Effect of degree of superheat for liquid of $Pr \ll 1$, on (a) Δ, (b) δ_m, (c) ζ, (d) ratio of Nu_x to Nu_x^0.

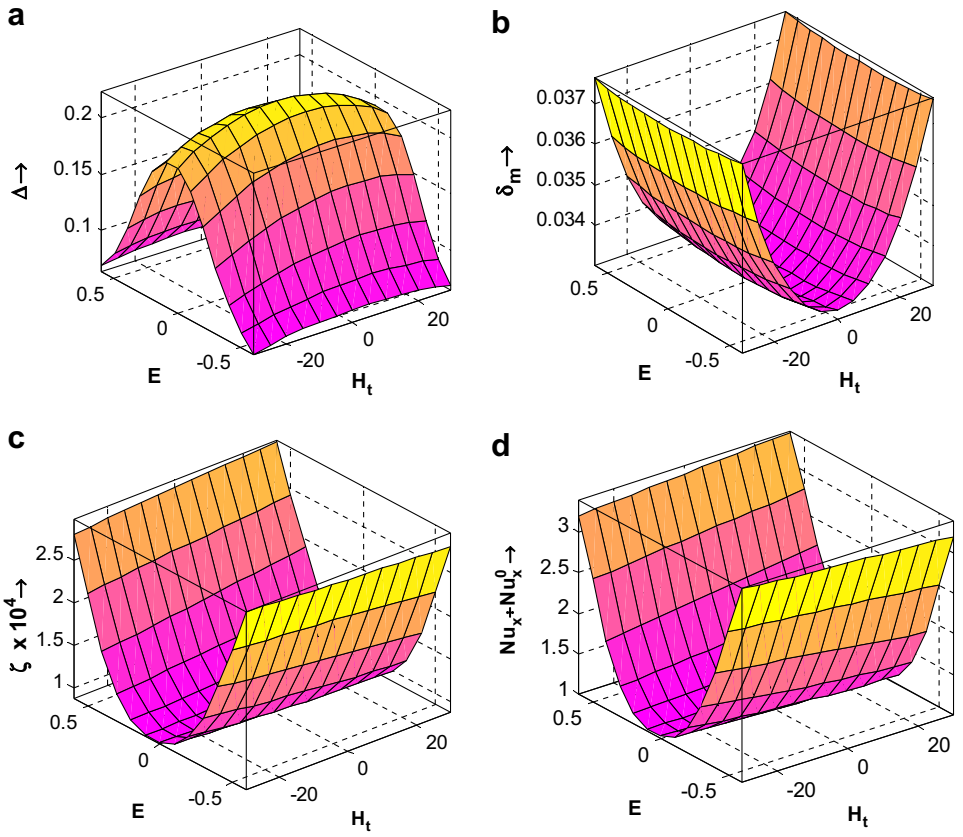

Fig. 5. Effect of combined electric and magnetic field for liquid with $Pr \gg 1$ at a location $x = 0.5$ on (a) Δ – ratio of boundary layer thickness, (b) δ_m – normalized momentum boundary layer thickness, (c) ζ – interface velocity, (d) ratio of Nu_x to Nu_x^0.

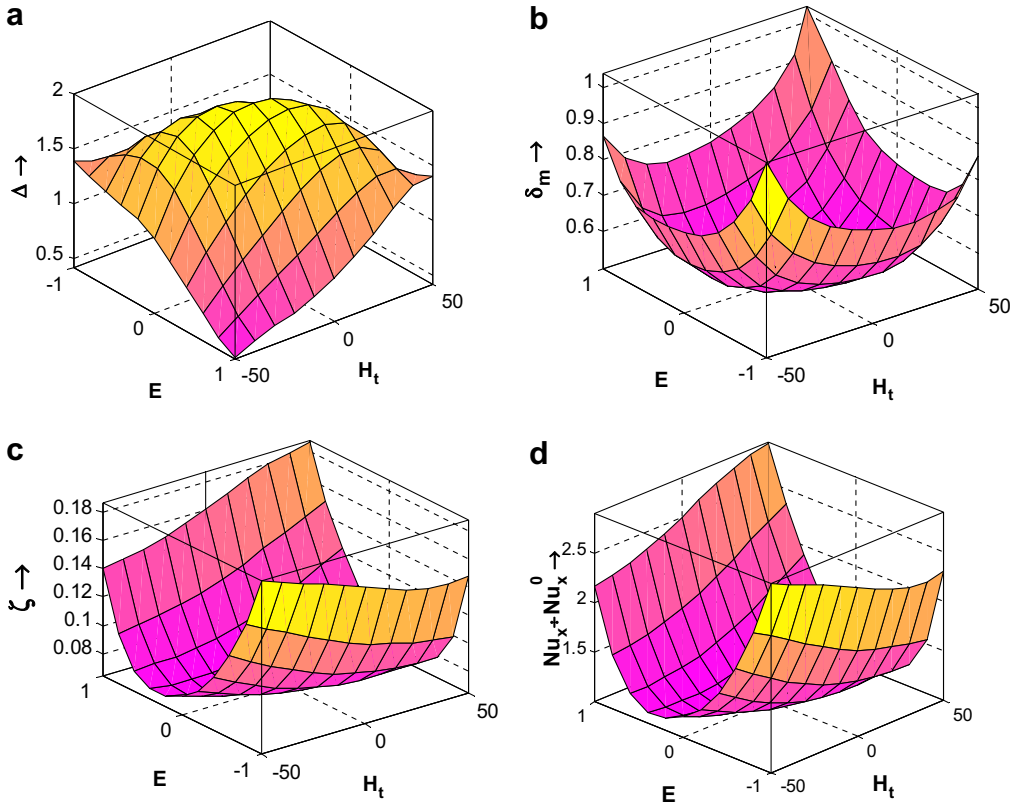

Fig. 6. Effect of combined electric and magnetic field for liquid with $Pr \ll 1$ on (a) Δ – ratio of boundary layer thickness, (b) δ_m – normalized momentum boundary layer thickness, (c) ζ – normalized interface velocity, (d) ratio of Nu_x to Nu_x^0.

3.2.2. Effect of electric and magnetic fields

Apart from degree of superheat, the electric fields and magnetic fields are likely to bear significant consequences with regard to the transport phenomena associated with the melting process. Figs. 5 and 6 depict the combined influences of the electric and magnetic fields on the various characteristics of the melting process, for $Pr \gg 1$ and $Pr \ll 1$ respectively. All these variations are plotted corresponding to an axial location given by $x = 0.5$. It is important to recognize in this context that the magnetic field influences the momentum and thermal energy transport simultaneously. However, the electric field does not explicitly influence the momentum transport, although it significantly influences the thermal energy transport by contributing to the Joule heating. Accordingly, it is revealed from Fig. 5a and b that the thermal and hydrodynamic transport are almost decoupled. A weaker flow field that is established on account of the application of magnetic fields becomes responsible for an effective retardation in the advective transport of momentum, leading to a thickening of the hydrodynamic boundary layer thickness. While the effects of variations in M (or equivalently H_t) are exhibited to be prominent only for their implications on δ_m, variations in E additionally influence the values of Δ, melting rate and ratio of Nusselt numbers, as evident from Fig. 5, because of the explicit contributions of the electric field on Joule heating.

For $Pr \ll 1$ (see Fig. 6), the effects on the melting parameters are found to be prominent for both the electric and magnetic fields, in sharp contrast to the cases with $Pr \gg 1$. It should be noted that even though the thermal gradient is less in case of $Pr \ll 1$ (because of thicker thermal boundary layer), the increased value of thermal conductivity causes higher heat flux to flow into the solid, resulting in higher rates of melting. This is aptly justified from Figs. 5c and 6c, which reveal considerably higher rates of melting for $Pr \ll 1$. Appreciably high rates of melting for $Pr \ll 1$ effectively 'pump' fresh layers of molten liquid into the boundary layer, so that the rates of momentum transfer are also implicitly influenced. Accordingly, the melting characteristics of low Prandtl number fluids are simultaneously influenced by both M (or equivalently H_t) and E.

With regard to the variations in Nusselt number, it first needs to be recognized that the Nusselt number is nothing but a non-dimensional measure of the convective heat flux, which strongly depends on the volumetric rate of heat generation due to Joule heating. From Eq. (6) it is revealed that the above scales as, $S \sim \left(E + U \cdot M\sqrt{Ec}\right)^2$. The strength of this volumetric heating not only depends on the strengths of the electric and the magnetic fields, but also on their relative algebraic signs. When both E and M (or equivalently H_t) are of the same sign, their combined influences enhance the strength of volumetric heating. On the other hand, when these are of opposite sign, the strength of the source weakens. The strength of the source is a minimum when neither the electric field nor the magnetic field is applied. With high strengths of this source, an enhanced rate of volumetric heat generation tends to overweigh the effects of thermal diffusion, so as to render the thermal boundary layer thinner. Thinner the thermal boundary layer, steeper is expected to be the temperature gradient within the same. As a result, the heat flux available for the solid–liquid phase transition increases, which implies an augmentation in the rate of melting. This, in turn, is accompanied with an enhancement in the Nusselt number, all other conditions remaining unaltered. Thus, a combination of the strongest magnetic field and the strongest electric field, within the chosen regime, results in the maximum possible rate of melting and also the maximum possible value of Nusselt number, provided both are of the same sign, as apparent from Fig. 6c and d. Interestingly, the rate of melting and the overall rate of convective transport turn out to be some-

what less when fields of the same strength but of opposite algebraic sign are employed, for reasons mentioned earlier. When the magnetic and electric fields act in tandem and are of opposite sign, the maximum thermal boundary layer thickness (or equivalently, the minimum rate of melting) occurs when $|E| \sim \left|M\sqrt{Ec}\right|$, which is essentially a scaling limit at which the volumetric energy generation rate on account of Joule heating tends to zero.

4. Conclusions

In this paper, a semi-analytical approach has been outlined to analyze the fundamental physical principles of controlling various aspects of melting in forced flows through combined electro-magneto-hydrodynamic influences. This study has been motivated by the fact that the application of electro-magnetic fields has now become widely practiced in the materials processing industries, so as to obtain improved product qualities through the imposition of stringent process control mechanisms. Although, because of distinctive development histories and different quality requirements, the metal and semiconductor researchers have contrasting focuses in their research on melting/solidification processing in electromagnetic fields, the fundamental design principles to be applied are expected to be essentially the same. Metals researchers, while perfecting the standard practices, are continuously exploring the possibilities of extending the use of the electromagnetic fields in near-net-shape casting, thin-gauge casting, and other novel casting processes. On the other hand, the crystal growers are routinely preoccupied with adapting electromagnetic stirring in semiconductor melts while developing more effective and efficient magnetic damping field configurations. The present study, through its fundamental physical considerations, is expected to cater these diverse requirements through a unified approach. From the simulation case studies undertaken on the basis of the boundary layer integral model developed here, the following important conclusions can be drawn in this regard:

1. The effect of the applied electric and magnetic field is inconsequential at the leading edge of the plate and becomes progressively more important as one traverses along the length of the slab. Thus, the ratio of Nusselt number with and without the employment of electromagnetic field increases almost linearly along the slab length.
2. Increase in degree of superheat of the liquid augments the rate of melting. However, the degree of superheat in the liquid appears to be rather inconsequential in influencing the hydrodynamic and the thermal boundary layer thicknesses.
3. Appreciable influences of the electric and magnetic fields can be observed with regard to the variations in the local boundary layer thicknesses, melting rate and the Nusselt number. While favorable combinations of the electric and the magnetic fields (both being of same algebraic sign) may improve the rate of melting and the consequent rate of convective transport to a significant extent, their opposing combinations with the electric and magnetic fields of contrasting sign can reduce the corresponding rates to considerable proportions. The underlying influences are much more dramatic for low Prandtl number fluids than the high Prandtl number ones. In practice, therefore, judicious combinations of the magnetic and electric field can be employed to control the rate of melting and the pertinent rate of convective heat transfer, for a chosen type of phase changing material.

Appendix A. Specification of parameters appearing in Eqs. (18)–(20)

	Eq. (18)	Eq. (19)	Eq. (20)
c_1	$\frac{9}{70}(\phi+1)-\frac{12}{35}\phi^2$	$6\phi Z+\left(\frac{1}{5}-\frac{b_1}{20}\right)\Delta^3-\left(\frac{1}{14}-\frac{2b_1}{105}\right)\Delta^4$	$6\phi Z+\frac{1}{\Delta^3}\left[-\left(\frac{1}{14}-\frac{b_1}{28}\right)+\left(\frac{1}{5}-\frac{2b_1}{15}\right)\Delta+\frac{3b_1}{20}\Delta^2-\frac{1}{2}\Delta^3+\left(\frac{1}{2}-\frac{b_1}{12}\right)\Delta^4\right]$
c_2	$\frac{1}{35}M^2Re\phi\left(\frac{3}{4}-4\phi\right)$	$M^2Re\phi Z$ where $Z=\left(\frac{3}{20}-\frac{b_1}{30}\right)\Delta^2-\left(\frac{2}{15}-\frac{b_1}{30}\right)\Delta^3+\left(\frac{1}{28}-\frac{b_1}{105}\right)\Delta^4$	$M^2Re\phi Z$ where $Z=\frac{1}{\Delta^3}\left[\left(\frac{2}{105}-\frac{b_1}{105}\right)-\left(\frac{1}{20}-\frac{b_1}{30}\right)\Delta-\frac{b_1}{30}\Delta^2+\frac{\Delta^3}{12}\right]$
c_3	$-\frac{1}{105}(M^2Re\phi)^2$	–	–
d_1		$-\frac{1}{35}\Delta[35e^2+M^2\Delta^4(63-70\Delta+20\Delta^2)-35Me\Delta^2(\Delta-2)-35Me\Delta\psi_1\phi+M^2\Delta^3\psi_2\phi+12M^2\Delta^4\psi_3\phi^2]$	$-\frac{1}{35}[35\Delta(M+e)^2-35Me(1-\phi)+M^2(2+\phi)(12\phi-11)]$
d_2		$-\frac{1}{210}M^3Re\phi\Delta^2[35e\psi_1-M\Delta^2\psi_2+24M\Delta\psi_3\phi]$	$-\frac{1}{210}M^3Re\phi[35e+13M+24M\phi]$
d_3		$-\frac{M^6Re^2\phi^2\Delta^3}{105}\psi_3$ where $\psi_1=6-8\Delta+3\Delta^2$, $\psi_2=-315+672\Delta-490\Delta^2+120\Delta^3$, $\psi_3=35-105\Delta+126\Delta^2-70\Delta^3+15\Delta^4$	$-\frac{M^6Re^2\phi^2}{105}$

References

[1] D.A. Shtanko, Solidification of steel in a magnetic field, Zh. Tekh. Fiz. 3 (6) (1933) 1085.
[2] A. Bruchanov, Solidification of steel in a rotating magnetic field, Stahl Eisen 54 (1934) 1111.
[3] E. Takeuchi et al., Applied MHD in the process of continuous casting, in: J. Szekely et al. (Eds.), Magnetohydrodynamics in Process Metallurgy, TMS, Warrendale, PA, 1992, pp. 189–202.
[4] S. Asai, in: J. Lielpeteris, R. Moreau (Eds.), Metallurgical Aspects of Electromagnetic Processing of Materials in Liquid Metal Magnetohydrodynamics, Kluwer Academic Publishers, Boston, MA, 1989.
[5] R.W. Series, D.T. Hurle, The use of magnetic fields in semiconductor crystal growth, J. Cryst. Growth 113 (1991) 305–328.
[6] G. Müller, Convection and inhomogeneities in crystal growth from the melt, in: H.C. Freyhardt (Ed.), Crystal: Growth, Properties and Applications, vol. 12, Springer-Verlag, Berlin, 1988.
[7] G.M. Oreper, J. Szekely, The effect of a magnetic field on transport phenomena in a Bridgman–Stockbarger crystal growth, J. Cryst. Growth 67 (1984) 405–419.
[8] S. Motakef, Magnetic field elimination of convective interference with segregation during vertical-Bridgman growth of doped semiconductors, J. Cryst. Growth 104 (1990) 833–850.
[9] D.H. Kim, P.M. Adornato, R.A. Brown, Effect of vertical magnetic field on convection and segregation in vertical Bridgman crystal growth, J. Cryst. Growth 89 (1988) 339–356.

[10] H.B. Hadid, D. Henry, Numerical study of convection in the horizontal Bridgman configuration under the action of a constant magnetic field. 1. Two-dimensional flow, J. Fluid Mech. 333 (1997) 23–56.
[11] D. Xu, Y. Bai, H. Fu, J. Guo, Heat, mass and momentum transport behavior in directionally solidifying blade-like castings in different electromagnetic fields described in a continuum model, Int. J. Heat Mass Transfer 48 (2005) 2219–2232.
[12] S. Kaddeche, H.B. Hadid, D. Henry, Macrosegregation and convection in the horizontal Bridgman configuration. I. Dilute alloys, J. Cryst. Growth 135 (1994) 341–353.
[13] K.I. Fedoseyev, E.J. Kansa, C. Martin, A.G. Ostrogorsky, Magnetic field suppression of semiconductor melt flow in crystal growth: comparison of three methods for numerical modeling, Jpn. CFD J. 9 (2000) 325–333.
[14] P.A. Davidson, Magnetohydrodynamics in materials processing, Ann. Rev. Fluid Mech. 31 (1999) 273–300.
[15] B.H. Dennis, G.S. Dulikravich, Simulation of magnetohydrodynamics with heat transfer, in: E. Onate, G. Bugeda, B. Suarez (Eds.), ECCOMAS2000 (European Congess on Computational Methods in Applied Sciences and Engineering), Barcelona, Spain, September 11–14, 2000.
[16] B.Q. Li, The fluid flow aspects of electromagnetic levitation processes, Int. J. Eng. Sci. 32 (1994) 45–67.
[17] G.S. Dulikravich, S.R. Lynn, Unified electromagneto-fluid dynamics (EMFD): a survey of mathematical models, Int. J. Non-Linear Mech. 32 (1997) 923–932.
[18] H.J. Ko, G.S. Dulikravich, A fully non-linear model of electro-magneto-hydrodynamics, Int. J. Non-Linear Mech. 35 (2000) 709–719.
[19] R.D. Cess, Magnetohydrodynamic effects upon heat transfer for laminar flow across a flat plate, ASME J. Heat Transfer 82 (1960) 87–93.
[20] M.H. Cobble, Magnetofluiddynamic flow with a pressure gradient and fluid injection, J. Eng. Math. 11 (1977) 249–256.
[21] W.C. Moffat, Analysis of MHD channel entrance flow using the momentum integral method, AIAA J. 2 (1964) 1495–1497.
[22] W.H. Heiser, W.J. Bornhorst, A modified Pohlhausen velocity profile for MHD boundary layer problems, AIAA J. 4 (1966) 1139–1141.
[23] M. Epstein, D.H. Cho, Melting heat transfer in steady laminar flow over a flat plate, ASME J. Heat Transfer 98 (1976) 531–533.
[24] O.M. Griffin, Heat, mass and momentum transfer during the melting of glacial ice in sea water, ASME J. Heat Transfer 95 (1973) 317–323.
[25] V. Seeniraj, N.P. Kannan, Magnetic field effects upon heat transfer for laminar flow of electrically conducting liquid over a melting slab, Int. J. Heat Mass Transfer 46 (2003) 1599–1605.